

# Quantitative interpretation of multi-spectral fundus images

I. B. Styles<sup>a</sup>, E. Claridge<sup>a</sup>, F. Orihuela-Espina<sup>a</sup>, A. Calcagni<sup>a,b</sup>, J. M. Gibson<sup>b</sup>

<sup>a</sup>School of Computer Science, The University of Birmingham, Edgbaston, Birmingham, B15  
2TT, United Kingdom.

<sup>b</sup>Birmingham and Midland Eye Centre, City Hospital NHS Trust, Dudley Road, Birmingham,  
B18 7QU, United Kingdom

## ABSTRACT

Multi-spectral imaging of the ocular fundus suffers from three main problems: the image must be taken through an aperture (the pupil), meaning that the absolute light intensity at the fundus cannot be known; long acquisition times are not feasible due to patient discomfort; patient movement can lead to loss of image quality. These difficulties have meant that multi-spectral imaging of the fundus has not yet seen wide application.

We have developed a new method for optimizing the multi-spectral imaging process which also allows us to derive semi-quantitative information about the structure and properties of the fundus. We acquire images in six visible spectral bands and use these to deduce the concentration and distribution of the known absorbing compounds in the fundus: blood haemoglobins in the retina and choroid, choroidal melanin, RPE melanin and xanthophyll.

The optimisation process and parameter recovery uses a Monte Carlo model of the spectral reflectance of the fundus, parameterised by the concentrations of the absorbing compounds. The model is used to compute the accuracy with which the values of the model parameters can be deduced from an image. Filters are selected to minimise the error in the parameter recovery process.

Theoretical investigations suggest that parameters can be recovered with RMS errors of less than 10%. When applied to images of normal subjects, the technique was able to successfully deduce the distribution of xanthophyll in the fundus. Further improvement of the model is required to allow the deduction of other model parameters from images.

**Keywords:** multi-spectral, ocular fundus, quantitative, biomedical optics, Monte Carlo

## 1. INTRODUCTION

Recent innovations in imaging technology have led to a surge of interest in hyper- or multi-spectral images. Conventional RGB digital images consist of three superposed images taken using broad-band red, green and blue filters. They provide excellent spatial resolution but very low spectral resolution, making it very hard to determine precisely what physiological or histological feature is causing a particular feature in an image. In contrast, traditional tissue spectroscopy can allow us to deduce detailed information about the properties of tissue at a given point, but it does not allow us to examine the properties of large areas of tissue. We conclude that neither of these techniques is necessarily optimal for screening and diagnostic purposes.

In theory, multi-spectral imaging combines the spatial resolution of conventional colour images with the spectral detail usually associated with spectroscopy. Such images are usually composed of a number of images taken using a pre-determined set of narrow-band filters which provide the desired level of spectral detail. Several methods exist for acquiring such images. The most common is to simply take pictures using individual filters and combining them to form the multi-spectral images. More recently, a number of groups have used programmable filters. These use LCD technology to allow a single device to be programmed to implement a wide range of narrow-band filters, simplifying the acquisition process by virtue of needing only one physical device. Finally, there are so-called hyper-spectral imaging systems which use interferometric methods to construct spectra at each point in an image.

---

Email correspondence to IBS at I.B.Styles@cs.bham.ac.uk

One drawback of these systems is that multi-/hyper-spectral image acquisition can be a time-consuming process, depending on the level of spectral resolution required. For exposed surfaces where the tissue is readily accessible and can be easily immobilised, this is not necessarily a prohibitive difficulty; but for less accessible tissues this is a particular problem. The application that concerns us in this paper is that of ocular fundus imaging, where an extended acquisition time can lead to three major difficulties:

1. Patient discomfort, caused by exposure to an illuminating light source for extended periods of time
2. Misalignment of images, caused by involuntary movements of the ocular fundus (the so-called "saccades"). This can be compounded by the length of the exposure, but can be corrected by registration of the images.
3. Movement of the subject can lead to loss of image quality if the exposure times are long

There is hence a requirement for the imaging process to be optimised in order to minimise these problems, but the resulting multi-spectral images must still contain sufficient spectral detail to be diagnostically useful. In this paper we describe how we use the physical properties of normal tissue to determine a set of narrow-band filters which allow us to extract detailed information about the structure and properties of the tissues comprising the ocular fundus.

The key idea behind our technique is that epithelial tissues, including the ocular fundus, all have a fairly regular layered structure. Each layer of the structure contains a variety of different substances which each interact with light in different ways. In particular, each component of the tissue can absorb and scatter light. By modelling the interaction of the illuminating light with a range of different tissue compositions, we construct a model of tissue reflectance which describes the range of colours which we would expect to see in normal tissue. Points in the image which have a colour lying outside the model can be identified and investigated further using more specialised techniques such as fluorescein angiography or optical coherence tomography (OCT).

Such ideas are not new: essentially the same idea is used in the SIAScope system used to screen for skin cancer.<sup>1</sup> This system uses the standard RGB filters plus an additional infrared filter to analyse and decompose the structure of the skin, and can identify the abnormal structures which are characteristic of malignant skin tumours.<sup>2</sup> However, the development of the technique for use in the ocular fundus is rather less straightforward than one might imagine. Firstly, the structure of the fundus tissues is much more complex than that of the skin, and there are many more optically important histological components. Secondly, the fact that images of the fundus are always taken through a small aperture (the pupil) means that one cannot control exactly the amount of light that reaches the fundus. This means that the images cannot be calibrated using simple patches of known reflectance placed near the sample site. Thirdly, the resulting model of tissue colouration is non-linear making the interpretation of the images very hard. Finally there is the problem of obtaining appropriate images. A set of filters is required which allows properties of the model to be deduced with the greatest accuracy possible. A procedure for deducing such a set of filters, together with a method for dealing with the lack of calibration data was outlined by Preece and Claridge.<sup>3</sup> In this paper we show how to apply these ideas to imaging of the ocular fundus, and we present preliminary results obtained recently.

## 2. METHODS

### 2.1. Modelling the reflectance of the ocular fundus

It is well known that the appearance of biological tissue in medical images is governed by the interaction of the illuminating light with the tissue. Tissue can both absorb and scatter light in varying amounts, depending on the tissue's composition and structure. The interaction of light with tissue is governed by the radiative transport equation which is generally very hard to solve. Analytical solutions to the transport equation are known only for a very few rather simple situations, and these are not very useful when analysing complex structures such as those which can be found in the epithelial tissues. Fortunately there are a variety of approximations of differing accuracy which can be used to predict the optical transport properties of biological tissue. The simplest approximation scheme is known as the Kubelka-Munk model, which assumes that transport is essentially one-dimensional. It is known that this is a very crude approximation which does not always describe transport very well. A more

sophisticated method which we make use of in this work is the Monte Carlo numerical approximation method. This is a stochastic method which solves the transport equation numerically. It can achieve arbitrary levels of accuracy at the expense of long computation times. Several groups have used the Monte Carlo method to model the transport of light in the ocular fundus,<sup>4,5</sup> and have reported good results.

We have chosen to base our modelling on the work of Preece and Claridge.<sup>5</sup> They used the Monte Carlo code written by Jacques and Wang<sup>6,7</sup> to attempt to reproduce experimental spectra obtained from normal fundi.<sup>8</sup> Their basic assumption was that the ocular fundus can be modelled as a layered tissue, comprising of four principal layers: the retina (or nerve fibre layer); the retinal pigment epithelium (RPE); the choroid; and the sclera. Each of these layers is composed of some underlying structural tissue which is known to scatter light, combined with additional pigmented compounds such as melanin and haemoglobins. They assumed that the optical properties of the underlying tissues would remain constant, as was suggested by Hammer *et al.*<sup>4</sup> and that variations in the appearance of ocular fundi (both inter- and intra-subject) were due solely to variations in the quantity of pigmented compounds present. The pigments considered by Preece and Claridge were: melanins in the RPE; haemoglobins in the choroid; and melanins in the choroid.

The investigations of Preece and Claridge were aimed at predicting the appearance of perifoveal areas of the fundus. It is known that the foveal areas of the fundus contain an additional absorbing compound, xanthophyll,<sup>9</sup> which must also be included if we also wish to model the foveal region. In addition, we found that it is necessary to model the effect of haemoglobins in the retina (assuming 80% oxygenation) in order to accurately reproduce experimental data in many areas of the fundus. Accordingly, we constructed a model of fundus reflectance described by five parameters:

1. Haemoglobins in the retina
2. Xanthophyll in the retina
3. Melanin in the RPE
4. Haemoglobins in the choroid
5. Melanin in the choroid

We assume that other physical properties (e.g. thickness) of the tissue have the constant values found by Preece and Claridge,<sup>5</sup> and that the absorption and scattering properties of the underlying tissue are constant, as found by Hammer *et al.*<sup>4</sup>

Having identified the variables that parameterise the model it is straightforward to compute the reflectance spectrum of the tissue for any combination of parameters. Parameter ranges were chosen according to a mixture of published normal ranges taken from Preece and Claridge<sup>5</sup> (and references therein); and by examining the effect of each parameter on the reflectance spectrum: at large values, changing a parameter has little effect on the reflectance. The effect of each model parameter on the reflectance spectra is shown in Fig. 1.

## 2.2. Theoretical analysis of the imaging process

In principle, we could use this model to deduce the physical properties of a hyper-spectral image of the fundus. By comparing each point in the image with the model, it is possible to determine (to within a certain error) the values of the parameters which best describe the tissue. By doing this at every point in the image one could then show how each parameter varies across the fundus. However, we have already discussed some of the difficulties in obtaining hyper-spectral fundus images, and such a technique would certainly not be viable in a clinical setting using current imaging technologies. One important feature of our model is that it is parameterised by a set of just five variables, and so in principle, one needs only to measure the reflectance of the fundus at five wavelengths in order to be able to deduce which combination of parameters describes the tissue. Let us define the problem more formally.

We define a metric space  $\mathbf{P}$  containing all possible combinations of parameters describing the tissue. Each point in  $\mathbf{P}$  represents a unique combination of model parameters. Using Monte Carlo simulations, we define a

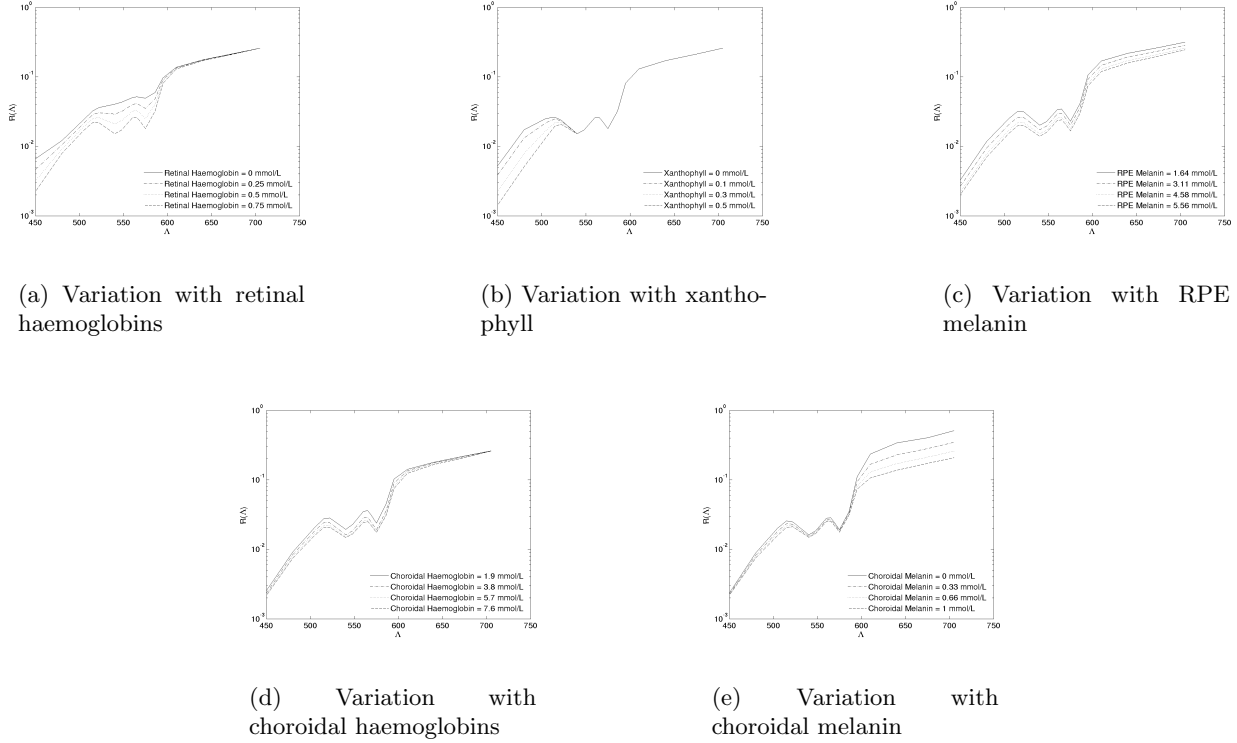


**Figure 1.** Some example spectra taken from our model of normal tissue. The non-varying parameters were fixed at: Retinal Haemoglobins = 0.75 mmol/L; Xanthophyll = 0.3 mmol/L; RPE Melanin = 4.58 mmol/L; Choroidal Haemoglobins = 5.70 mmol/L; Choroidal Haemoglobin = 0.66 mmol/L.

mapping  $s$  which takes us from parameter space  $\mathbf{P}$  onto “spectral space”  $\mathbf{S}$ :  $s : \mathbf{P} \mapsto \mathbf{S}$ . The spectral space can then be mapped onto so-called “image space”  $\mathbf{I}$  using a mapping  $i : \mathbf{S} \mapsto \mathbf{I}$ . The form of this mapping depends on the imaging technique. For laser imaging, one would simply select the appropriate wavelengths from the spectra, whereas if the images are obtained using filters, the spectra must be convolved with the filter response functions. For a set of filters  $F = \{F^1(\lambda), \dots, F^N(\lambda)\}$ ,  $i$  is defined as

$$i^n(\mathbf{x}) = \int_{\Lambda} R(\mathbf{x}, \lambda) I(\mathbf{x}, \lambda) F^n(\lambda) d\lambda, \quad (1)$$

where  $I(\mathbf{x}, \lambda)$  is the spectral definition of the illuminant at spatial location  $\mathbf{x}$ ,  $R(\mathbf{x}, \lambda)$  is the spectral reflectance of the tissue at wavelength  $\lambda$ , position  $\mathbf{x}$ , and the  $i^n(\mathbf{x})$  are the “image values” which comprise the image (for example, the red, green and blue values that define an RGB image). An important feature of this equation is the spatial dependence of the illuminant. This is particularly important for fundus images, where the image is taken through an aperture (the pupil). This means that the illumination of the fundus is always uneven, being darker at the edges due to vignetting at the pupil. Normally, one would place a calibration patch on the surface of the object being imaged in order to determine the variation of illumination with position, but this is clearly not possible for the fundus. Fortunately, there is no reason to expect the spatial distribution of the illuminant to vary with wavelength, and so we may separate  $I(\mathbf{x}, \lambda)$  into spatial and spectral components:  $I(\mathbf{x}, \lambda) = A(\mathbf{x}) S(\lambda)$ . We can then rewrite Eqn. (1) as

$$i^n(\mathbf{x}) = A(\mathbf{x}) \int_{\Lambda} R(\mathbf{x}, \lambda) S(\lambda) F^n(\lambda) d\lambda, \quad (2)$$

and  $A(\mathbf{x})$  can then be eliminated by taking the ratio of two image values to give *image quotients*  $q_{mn}(\mathbf{x}) =$

$i_m(\mathbf{x})/i_n(\mathbf{x})$ . This defines a mapping  $q : \mathbf{I} \mapsto \mathbf{Q}$  which maps image space onto quotient space.

We can now define a composite mapping  $f = q \circ i \circ s : \mathbf{P} \mapsto \mathbf{Q}$  which maps model parameters onto image quotients. Each of the mappings which compose  $f$  can be computed quite simply:  $s$  is implemented using Monte Carlo simulations;  $i$  and  $q$  are very simple indeed. Hence for a given set of model parameters (tissue histology), we can compute the resulting image quotients. Both  $\mathbf{P}$  and  $\mathbf{Q}$  are vector spaces, and we will usually represent a point in parameter space as a vector  $\mathbf{p}$ , and a point in the quotient space as a vector  $\mathbf{q}$ , such that  $\mathbf{q} = \mathbf{q}(\mathbf{p})$ .

Since our objective is to be able to deduce the vector  $\mathbf{p}$  from an image, we require the inverse mapping  $f^{-1} : \mathbf{Q} \mapsto \mathbf{P}$ . The construction of such a mapping is generally a very hard problem and there are no general methods. Indeed, the existence of  $f^{-1}$  is not guaranteed unless  $f$  itself has certain properties. We require that  $f$  must obey the inverse function theorem<sup>10</sup> which essentially states that in order for  $f^{-1}$  to exist,  $f$  must be “one-to-one” and “onto” (i.e. bijective). The condition that must be met in order for this to be guaranteed is that the Jacobian of  $f$  must be strictly positive or strictly negative at all points in the space. For our mapping, the components of the Jacobian matrix are defined as  $J_{ij} = \partial q_i / \partial p_j$ . The Jacobian is then  $\mathcal{J} = \det(\mathbf{J})$ . It is very straightforward to compute  $\mathcal{J}$  for every point in  $\mathbf{P}$  (we have discretized  $\mathbf{P}$ ) and to check whether  $\mathcal{J}$  changes sign. If it does, then the inverse mapping does not exist. If it does not, then the inverse can be computed in principle. An important consequence of this is that the Jacobian matrix must be square in order for the determinant to be non-zero (otherwise it is zero everywhere), and so vectors  $\mathbf{p}$  and  $\mathbf{p}$  must be of the same length. Therefore we require five independent image quotients in order to recover five model parameters. This means that we actually require *six* images in order to ensure that the quotients are independent. To see why this is true, note that the recovery of one parameter requires two images in order to be able to form the quotient. Similarly, recovering two parameters requires three images. If we were to try to form two quotients,  $q_1$  and  $q_2$  from two images  $i_1$  and  $i_2$  then we can only form  $q_1 = i_1/i_2$  and  $q_2 = i_2/i_1$ . Clearly  $q_1 = 1/q_2$ , and we can only really form one quotient from two images. If we introduce a third image  $i_3$ , then we can form  $q_1 = i_1/i_3$  and  $q_2 = i_2/i_3$ . To recover  $N$  parameters, we must take  $N + 1$  images.

Given the existence of both  $f$  and  $f^{-1}$ , we can then apply  $f^{-1}$  to an image in order to deduce the values of the model parameters which describe the tissue. The question then arises as to which images should we analyse? The forward mapping  $f$  is composed of a mapping from parameters to spectra, which is fixed: it is a model of the physics of light propagation in the tissue. The mappings  $i$  and  $q$ , which map us from reflectance spectra to image values and then to image quotients are not fixed: we have not specified which filters (or laser wavelengths) we should use to acquire the image; or which image values we should take ratios of to form the image quotients. We have the freedom to choose which images to acquire in order to optimise the recovery of parameters from an image. In an idealised situation, any set of filters and quotients which allow the model to be inverted would be sufficient, but in practise there are a variety of sources of error in both the model and in the image acquisition process. These will all combine to reduce the accuracy with which we can recover parameters from an image. We would like to choose a set of filters which minimise the errors with which parameters can be recovered, and so we want to be able to quantify the errors in the image analysis process. These errors arise from several sources. Sources of error in the forward model  $f$  are quite easily identified:

1. Measurement error in the data used to characterise the tissue: e.g. errors in absorption and scattering cross-sections.
2. Stochastic error in the Monte Carlo model of light propagation. This is inherent in Monte Carlo modelling.
3. Numerical error in the evaluation of Eqn. (2) due to the polynomial approximations inherent in numerical integration methods; and to the finite number of spectral points in  $R(\lambda)$  that can be generated by Monte Carlo.

It is a straightforward exercise in error analysis to propagate each of these errors through  $f$  to produce an estimate of the error with which each of the image quotients can be computed from a given set of parameters. We can then calculate the error in the inverse model, which tells us how accurately parameters can be recovered from a given set of quotients. In addition to these errors in the forward model there are also errors in the image acquisition process, typically due to random thermal noise in the CCD of the detector. These can be easily

combined with errors in the inverse model to obtain a measure of the overall error in the parameter recovery procedure. A full derivation of these results is beyond the scope of this paper; for further details, refer to the work of Preece and Claridge.<sup>3</sup>

Once a method for computing the error in parameter recovery has been established, a set of image quotients can be chosen which minimises this error. This is a non-trivial optimisation problem and we have elected to make use of recent advances in evolutionary optimisation methods to find optimal filters. Our algorithm of choice is due to Yao and Liu<sup>11</sup> and is a population-based evolutionary algorithm which finds the minimum in a given “fitness function” (in our case, the error in parameter recovery). In addition to the minimisation of the error, we must also test the Jacobian to ensure that the function is invertible, and we also place constraints on the filters that can be selected to ensure they can be implemented.

### 2.3. Image Acquisition

Imaging of the ocular fundus is a specialised procedure requiring high quality, specialised optics. The acquisition system used to obtain images for this work is based around a Zeiss RCM250 fundus camera which we have modified. The RCM250 uses a standard 35mm SLR to capture fundus images, and this is easily replaced by a digital imaging system consisting of:

- Retiga EXi 12-bit monochrome digital camera, with internal cooling (Qimaging, Canada).
- VariSpec tunable LCD optical filter (Cambridge Research Instruments, USA)
- Corrective optics

The Retiga EXi camera was chosen for its low-noise properties and high dynamic range. It is also extremely simple to program and control. The size of the CCD in the camera is only 1/3 inches, much smaller than the 35mm film for which the RCM250 was designed. The corrective optics were required in order to shrink the image from the camera to fit, and also to ensure that the image on the CCD and the image seen by the operator were parfocal. The VariSpec tunable filter from Cambridge Research Instruments is an LCD-based interference filter which can be programmed to pass a range of narrow bands. The pass-bands that can be programmed are approximately Gaussian in shape and are specified by the central wavelength only: the bandwidth and transmittance cannot be adjusted independently of the passband centre. Both the Retiga EXi camera and the VariSpec filter can be controlled by computer, and we have written simple software which acquires images using different filters in rapid succession.

Conventional fundus photography uses flash illumination to allow the fundus to be illuminated very brightly for a very short period of time. We have chosen not to use the flash capabilities of the RCM250 and instead to acquire images using the halogen viewing lamp that is normally used to aid positioning and focusing of the fundus camera. The reason for this choice is that the spectrum of the xenon flash lamp normally used in fundus photography is not smooth, containing several very sharp peaks and introducing significant errors in the evaluation of Eqn. (2). The peaks also tend to skew the filter optimisation process. In addition, the Monte Carlo modelling of light propagation assumes steady-state illumination rather than the transient illumination provided by the flash. We found that it was quite possible to obtain very good quality images without excessively long exposure times using this source of illumination.

### 2.4. Parameter Recovery

In Sect. 2.2 we showed how to construct a forward predictive model of the imaging process which allows us to compute the properties of an image given the properties of the fundus tissues. In order to be able to apply this model to the interpretation of fundus images we require the inverse mapping  $f^{-1}$  which allows us to compute the model parameters which best describe an image. We have shown how to deduce whether or not  $f^{-1}$  exists, but we have not shown how to construct it. It is clear that no analytical procedure exists for computing  $f^{-1}$  due to the numerically intensive nature of  $f$ . We have investigated several possibilities for implementing  $f^{-1}$ . During our studies, it emerged that the forward mapping  $f$ , and hence  $f^{-1}$  were both highly non-linear: in regions of  $\mathbf{P}$  where there are low concentrations of absorbers small changes in the concentrations lead to large changes

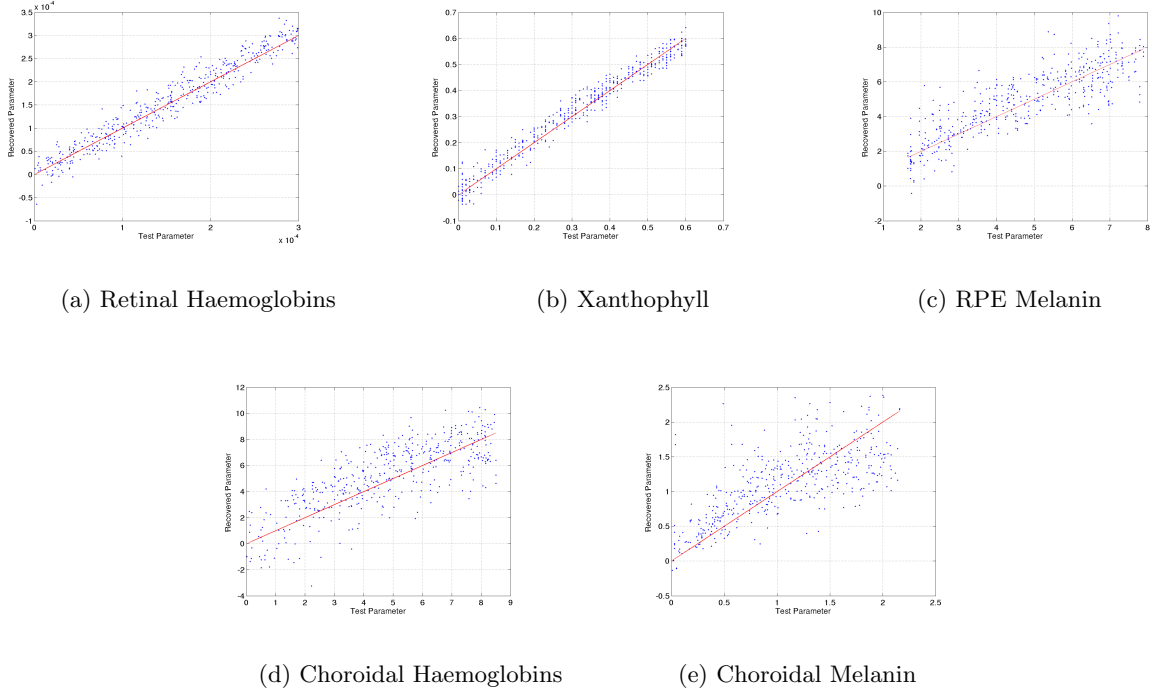


**Figure 2.** Results of parameter recovery on randomly generated data. Random parameter vectors were generated, the corresponding image quotients were computed and a neural network was used to recover the original parameter vector. The black line represents perfect parameter recovery; the blue points are the randomly generated parameters.

in the image quotients. Conversely, where there are high concentrations of absorbers, quite large changes in concentration cause very small changes in the image quotients. This is a natural consequence of the physics of light transport. This means that piecewise linear surface fitting does not give good results. We have found that the simplest and fastest method for computing  $f^{-1}$  is to use a neural network. We compute  $f$  for a large range of input parameter vectors, and we then pass these, plus the resulting image quotients to the neural network for training. The particular type of network used is the radial basis function network included in the MATLAB Neural Network toolkit which we have found to be both fast and easy to use. After training on the initial set of data, we tested the network on some random data. We generated a number of random points in  $\mathbf{P}$  and used these to compute the corresponding points in  $\mathbf{Q}$ . We then used the network to try to deduce the original points in  $\mathbf{P}$  using only the image quotients. The results of this are shown in Fig. 2.

It can be seen from Fig. 2 that not all parameters are recovered with equal accuracy: both xanthophyll (mean error:  $\pm 0.13\text{mmol/L}$ ) and retinal haemoglobins ( $\pm 0.37\text{mmol/L}$ ) are recovered with very good accuracy, but choroidal haemoglobins ( $\pm 3.7\text{mmol/L}$ ) and RPE and choroidal melanin ( $\pm 2.85\text{mmol/L}$ ,  $\pm 0.87\text{mmol/L}$ ) are not recovered so accurately. We are currently investigating ways of improving these results.

### 3. RESULTS

#### 3.1. Selection of optimal filters and model generation

Using the methods outlined in Sect. 2.2 we have computed filters which allow for the optimal recovery of model parameters from an image. These filters were selected subject to the constraints of our imaging equipment; that is, they must be implementable using the VariSpec filter. We therefore allowed the optimisation algorithm to vary only the central pass wavelength. This specifies all other properties of the filter. The optimisation algorithm was allowed to run until the results had converged, and this was repeated several times to guard against the

**Table 1.** Parameter values used to generate the forward model used for image interpretation.

Parameter	Values
Xanthophyll	{0.0, 0.1, 0.2, 0.3, 0.4, 0.5, 0.6} mmol/L
Retinal Haemoglobins	{0.0, 0.5, 1.0, 1.5, 2.0} mmol/L
RPE Melanin	{1.64, 3.11, 4.58, 5.56, 6.54, 8.00} mmol/L
Choroidal Melanin	{0.00, 0.33, 0.66, 1.00, 1.33, 1.66} mmol/L
Choroidal Haemoglobins	{1.90, 3.80, 5.70, 7.60, 8.50} mmol/L

possibility of finding only a local minimum. The filters selected had central wavelength at 507nm, 525nm, 552nm, 585nm, 596nm, with the extra filter used in the denominator of the image quotients being located at 611nm.

The filters were then applied (using Eqn. (2)) to a set of simulated reflectance spectra generated at points in  $\mathbf{P}$  defined by all possible combinations of the parameters shown in table 1. The resulting image values were then used to compute the image quotients corresponding to the original model parameters, defining the forward mapping  $f$ . The quotients and their corresponding parameters were then used to train a neural network to implement the inverse mapping  $f^{-1}$ .

### 3.2. Image acquisition

Images were acquired from a normal subject (with no known pathologies) using the optimal filters described in section 3.1. The subject was positioned appropriately and the fundus camera was positioned and focused by an experienced operator using a light level that was easily tolerated by the subject. Images were then acquired as 12-bit TIF images using the camera settings shown in table 2. These settings were found (after some experimentation) to produce good quality images without excessively long exposure times.

**Table 2.** Camera settings used to acquire fundus images.

Filter	Exposure Time	Camera Gain	Camera Offset	Binning Mode
507	1.2s	$\times 10$	+0	$2 \times 2$
525	0.6s	$\times 10$	+0	$2 \times 2$
552	0.45s	$\times 10$	+0	$2 \times 2$
585	0.15s	$\times 10$	+0	$2 \times 2$
596	0.075s	$\times 10$	+0	$2 \times 2$
611	0.050s	$\times 10$	+0	$2 \times 2$

The resulting raw images are shown in Fig. 3. The images were then registered to correct for small movements between the frames, and then corrected to account for the differing exposure times (all images were normalised to an exposure time of one second, unit gain, and zero offset). Following these corrections, the image quotients were calculated by dividing the image values at every pixel in each of the images by the value at the corresponding pixel in the image acquired at 611nm. The resulting image quotients correspond to the image quotients computed by the model.

### 3.3. Analysing the images

Before applying the neural network (inverse model) to the image quotients in order to deduce model parameters from the image, we compared the images with the model by hand in order to examine how well the model describes the real data. For each of the ten possible combinations of two image quotients, we projected both model and image data onto the corresponding plane. These projections are shown in Fig. 4. The projected data must be examined with extreme caution: even having the model and image data coincide in all projected views *does not guarantee* that they coincide in the five-dimensional space in which they reside. However, a poor match in any one of the projections *does* guarantee that the image and model data are different.

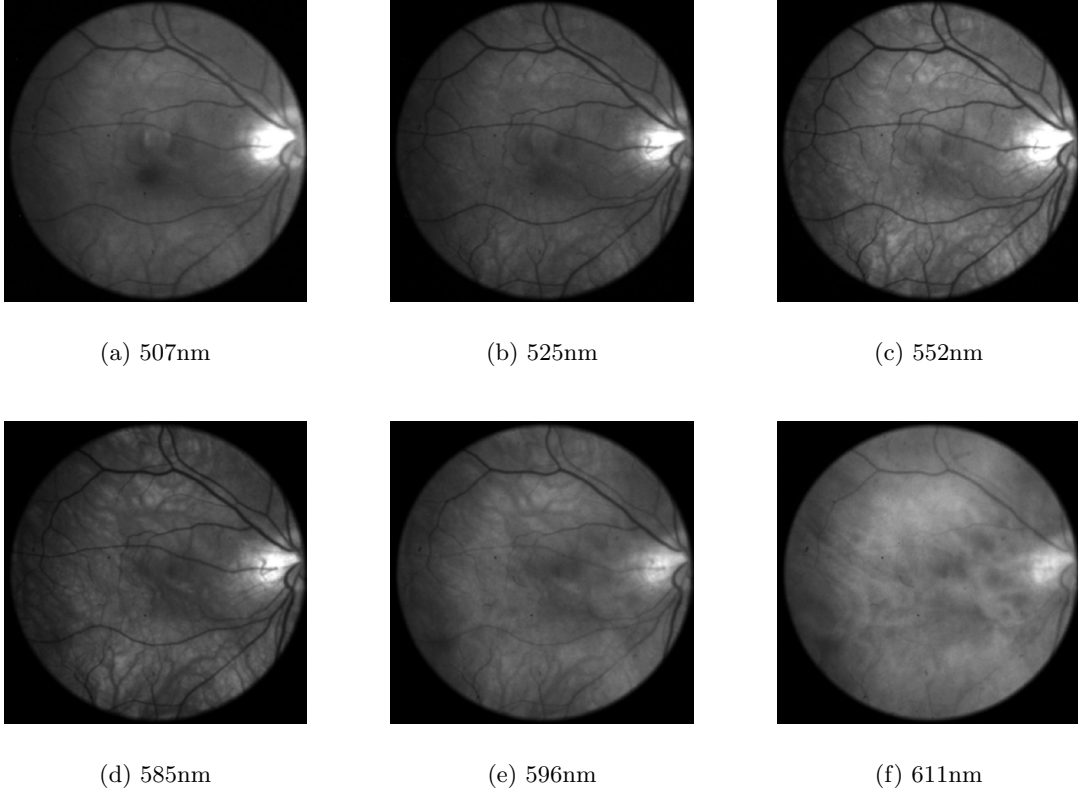


**Figure 3.** Raw image data acquired from a normal subject.

A careful analysis of the projected data leads us to several conclusions. Firstly we note that the wide variety of different shapes of the projected model data. In particular we note that several of the projections are very “thin”, suggesting quite strong correlations between the corresponding images. This is particularly noticeable in the projections onto the  $q_2-q_3$  and  $q_3-q_4$  planes, suggesting significant correlations between the images taken at 525nm and 552nm; and 552nm and 585nm. Pleasingly, we observe that the shape of the projected image data generally corresponds to the shape of the projected model data (i.e., when the projected model data is thin, so is the projected image data), suggesting that the quotients are similarly correlated in both model and image. In general we note that the projected model and image data are close, but do not necessarily match. We note especially that the projections onto the  $q_1-q_2$ ,  $q_1-q_3$  and  $q_2-q_3$  planes are all very well matched, but that projections onto the other planes are not. This is significant: the data in the numerator for each of these quotients  $q_1, q_2, q_3$  is taken from the green part of the visible spectrum, suggesting that the model describes the image quite well in this region. When we project onto planes corresponding to higher wavelengths, we observe that the model tends to overestimate the reflectance in the red.

The lack of complete correspondence between model and image data makes any further quantitative interpretation of the images very difficult. However, some simple investigations show that some further analysis is possible. An inspection of the absorption coefficient of xanthophyll reveals that it has no effect on light transport above 534nm. With this in mind, we attempted to recover the distribution of xanthophyll in the fundus using only  $q_1$ ,  $q_2$ , and  $q_3$ , where we have already observed that model and image data coincide in projected view. These quotients were used to train a neural network (as described in section 2.4) which was then applied to every point in the image data. The resulting distribution is shown in Fig. 5. The most notable feature of this picture is the significant increase in xanthophyll seen in the foveal region. This is a known feature of normal fundi and is as we expected. We also note that the points identified as lying outside the range of the model lie mainly in the area

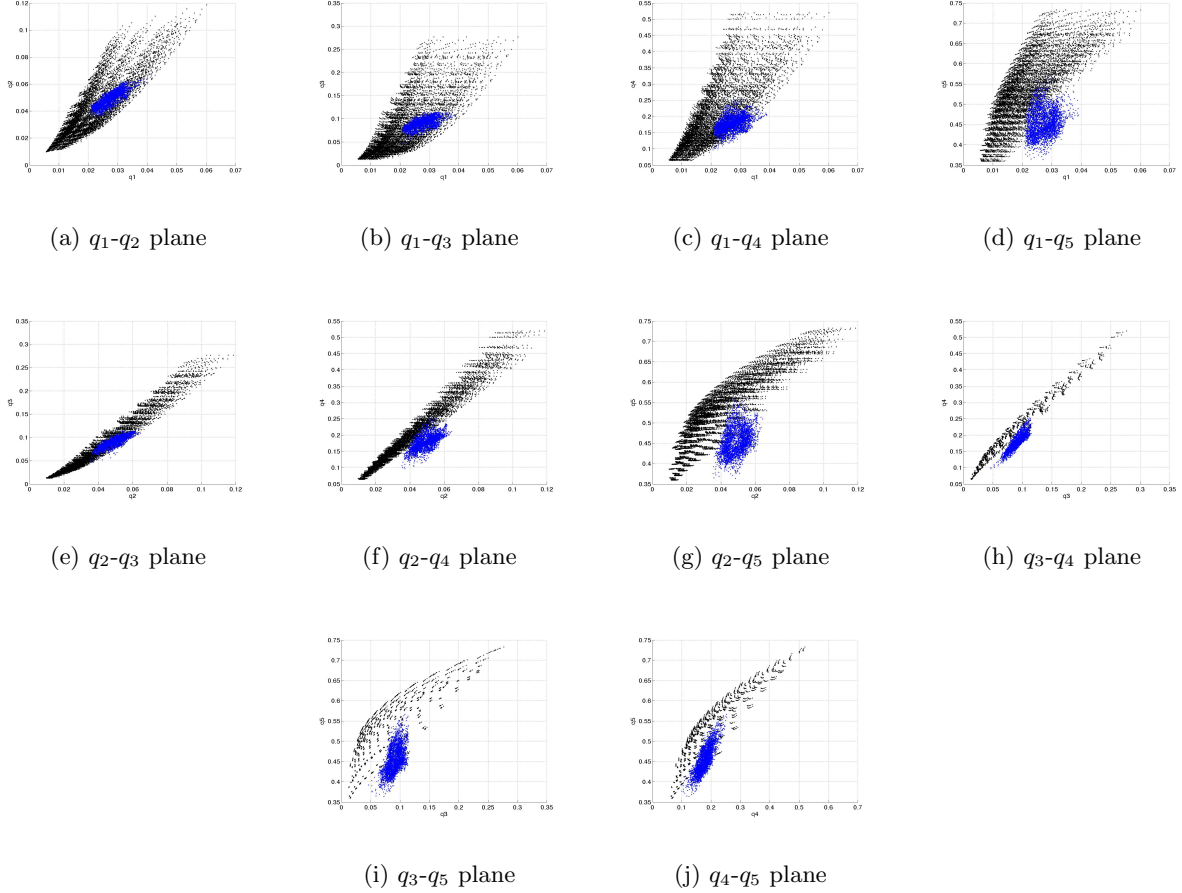


**Figure 4.** Projections of model quotients (black points) and image quotients (blue points) onto all possible planes, showing the correspondence between model data and image data. The quotients correspond to:  $q_1 = i(507\text{nm})/i(611\text{nm})$ ;  $q_2 = i(525\text{nm})/i(611\text{nm})$ ;  $q_3 = i(552\text{nm})/i(611\text{nm})$ ;  $q_4 = i(585\text{nm})/i(611\text{nm})$ ;  $q_5 = i(596\text{nm})/i(611\text{nm})$

of the disc (which we do not model), and on major retinal blood vessels, where we expect a higher concentration of haemoglobins than included in the model. These findings are in broad agreement with our expectations, and provide us with some optimism for the future success of these methods.

#### 4. DISCUSSION AND CONCLUSIONS

Although this work has yielded some promising results, especially with regard to the mapping of the distribution of xanthophyll within the ocular fundus, there are a number of significant non-trivial issues which must be addressed before we can progress further with this work. From an analysis of the projected image quotients shown in Fig. 4, it is clear that our current model of light propagation requires further development in order to improve the modelling of the image data in the red. We have identified several possible sources of improvement in this region. A recent paper<sup>12</sup> has suggested that the packaging of haemoglobins in erythrocytes has a very significant effect on the absorption spectrum. Furthermore, there may be effects due to absorption by other blood components, and we are investigating the effect of modelling whole blood instead of just haemoglobins. A further possibility is that there may be some direct reflection at the various surfaces in the optical path. Some studies<sup>8, 13</sup> have suggested that these may be important. There may also be some additional absorbing compounds which

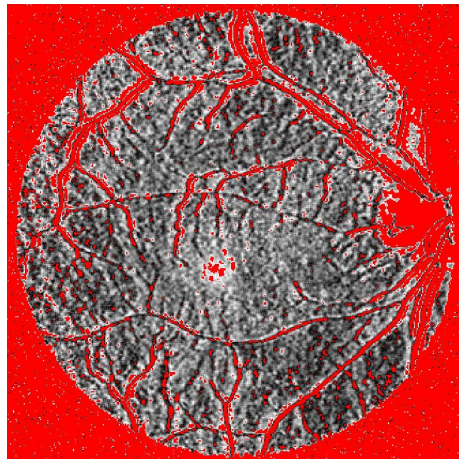


**Figure 5.** The distribution of xanthophyll in a normal fundus. Dark points indicate low levels of xanthophyll, light points indicate higher levels of xanthophyll. Red points indicate that the image data lies outside the range of the model data.

we have not included in the model, for example, lipofuscins. We will be attempting to characterise and model these in future work.

A rather more challenging possibility is that the modelling of light scattering in the fundus tissues is inadequate. The accuracy of our chosen Monte Carlo modelling technique is not in question: the key issue is the accuracy of the scattering cross-sections we are using to characterise the tissue. We have only identified one set of experimental measurements of scattering cross-sections of fundus tissues, namely those taken by Hammer *et al.*,<sup>4</sup> but some more recent work by some of the same authors has used optical coherence tomography (OCT) to suggest that the original measurements may have overestimated the scattering cross-section of choroidal tissue by up to a factor or two, at least in the infra-red (at 850nm). They attributed this difference to post-excision changes in the tissue in the original measurements, whereas the OCT measurements were performed *in vivo*. Recent work in our group<sup>14</sup> has successfully modelled the scattering properties of colon tissues from first principles and we will be investigating the application of similar ideas to fundus tissues.

As well as the scattering properties of the fundus tissues themselves we have also identified an additional source of scattering from erythrocytes and other blood components, and we are investigating how best to model this. Finally, there is an additional directional component to the tissue reflectance due to the light-guiding properties of receptor cells in the retina (the Stiles-Crawford effect).<sup>15–17</sup> It is not clear whether this is important for our purposes.

We conclude that whilst our initial results show some promise, the modelling of light transport in the fundus requires some significant changes, and we will be investigating a number of possible improvements which we outlined earlier. We will also continue to refine our techniques; a particular area which can be improved is the construction of the inverse mapping  $f^{-1}$ . We currently use a simple radial basis network to implement  $f^{-1}$ , but recent conversations with neural network experts suggest that significant improvements could be made in this area.

## ACKNOWLEDGMENTS

We acknowledge financial support from the EPSRC under grant number GR/S09906/01. We are especially grateful to Mr James Osborne for the generous donation of the Zeiss RCM250 fundus camera; and to Mr Peter Lundh of the Institute of Ophthalmology in London for his help in adapting the camera for use with digital image acquisition equipment.

## REFERENCES

1. E. Claridge, S. Cotton, P. Hall, and M. Moncrieff, "From colour to tissue histology: Physics based interpretation of images of pigmented skin lesions," *Medical Image Analysis* **7**, pp. 489–502, 2003.
2. M. Moncrieff, S. Cotton, E. Claridge, and P. Hall, "Spectrophotometric intracutaneous analysis - a new technique for imaging pigmented skin lesions," *British Journal of Dermatology* **146**, pp. 448–457, 2002.
3. S. J. Preece and E. Claridge, "Physics-based approach to geometry-insensitive recovery of quantitative scene parameters from images," Tech. Rep. CSR-04-08, University of Birmingham, School of Computer Science, 2004.
4. M. Hammer, A. Roggan, D. Schweitzer, and G. Muller, "Optical-properties of ocular fundus tissues - an *in-vitro* study using the double-integrating-sphere technique and inverse monte-carlo simulation," *Phys. Med. Biol.* **40**, pp. 963–978, 1995.
5. S. J. Preece and E. Claridge, "Monte carlo modelling of the spectral reflectance of the human eye," *Phys. Med. Biol.* **47**, pp. 2863–2877, 2002.
6. S. A. Prahl, M. Keijzer, S. L. Jacques, and A. J. Welch, "A monte carlo model of light propagation in tissue," *SPIE Institute Series IS* **5**, pp. 102–111, 1989.
7. L.-H. Wang, S. L. Jacques, and L.-Q. Zheng, "Mcml - monte carlo modeling of photon transport in multi-layered tissues," *Computer Methods and Programs in Biomedicine* **47**, pp. 131–146, 1995.
8. F. C. Delori and K. P. Pflibsen, "Spectral reflectance of the ocular fundus," *Appl. Opt.* **28**, pp. 1061–1077, 1989.
9. G. Wyszecki and W. S. Stiles, *Color Science: Concepts and Methods, Quantitative Data and Formulae*, Wiley, New York, second ed., 1982.
10. B. F. Schutz, *Geometrical Methods of Mathematical Physics*, Cambridge University Press, Cambridge, UK, 1980.
11. X. Yao and Y. Liu, "Fast evolution strategies," *Control and Cybernetics* **26**, pp. 467–496, 1997.
12. J. C. Finlay and T. H. Foster, "Effect of pigment packaging on diffuse reflectance spectroscopy of samples containing red blood cells," *Optics Letters* **29**, pp. 965–967, 2004.
13. R. W. Knighton, "Quantitative reflectometry of the ocular fundus," *IEEE Eng. Med. Biol.* **14**, pp. 43–51, 1995.
14. D. Hidovic and J. E. Rowe, "Validating a model of colon colouration using an evolution strategy with adaptive approximations," in *Genetic and Evolutionary Computation Conference*, pp. 414–427, 2004.
15. J. van de Kraats, T. Berendschot, and D. van Norren, "The pathways of light measured in fundus reflectrometry," *Vision Res.* **36**, pp. 2229–2247, 1996.
16. T. T. J. M. Berendschot, J. van de Kraats, and D. van Norren, "Wavelength dependence of the stiles-crawford effect explained by perception of backscattered light from the choroid," *J. Opt. Soc. Am. A-Opt. Image Sci. Vis.* **18**, pp. 1445–1451, 2001.
17. N. P. A. Zagers, T. T. J. M. Berendschot, and D. van Norren, "Wavelength dependence of reflectometric cone photoreceptor directionality," *J. Opt. Soc. Am. A-Opt. Image Sci. Vis.* **20**, pp. 18–23, 2003.